J. Phys. B: At. Mol. Opt. Phys. **32** (1999) 189–196. Printed in the UK PII: S0953-4075(99)95853-4

Production of Kr^{2+} and Kr^{0} in collision of Kr^{+} ions with Kr

H Martínez

Instituto de Física, Laboratorio de Cuernavaca, UNAM, Apdo Postal 48-3, 62251 Cuernavaca, Morelos, Mexico

Received 14 July 1998, in final form 1 September 1998

Abstract. Absolute differential and total cross sections for single-electron loss and capture were measured from Kr^{+} ions on Kr in the energy range of 1.0–5.0 keV. The reduced differential cross sections ($\rho = (d\sigma/d\Omega)\theta \sin\theta$) as a function of $\tau = E_{lab}\theta$ are shown to scale reasonably well for both products studied. For single-electron loss, our cross sections are found to be of the order of magnitude of 10^{-20} cm^2, while for single-electron capture the magnitude is 10^{-17} cm^2. The measured total cross sections are compared with theoretical models available in the literature.

1. Introduction

In an ion–atom collision, two of the basic processes present are single-electron capture and loss. The capture and loss of an electron by a fast ion upon colliding with an atom is one of the most typical phenomena accompanying the passage of fast atomic particles through matter. There are significantly few studies on Kr^{+} + Kr collisions and only very limited work on single-electron loss and capture processes. As examples of the limited literature we cite the experimental work of Barat *et al* (1970), who measured elastic and excitation differential cross sections on Kr^{+} + Kr at 0.8 and 1.05 keV. Their excitation-reduced cross sections show two successive crossings, with a first maximum at 1.13 keV deg and a second one at 2.3 keV deg, followed by some oscillations. Helm (1976) reported studies of the drift motion of Kr^{+} in a buffer gas of Kr. Their results show a dependence on the spin state of the ion and at thermal energies, the reduced zero-field mobilities of $Kr^{+}\left(^2P_{3/2}\right)$ and $Kr^{+}\left(^2P_{1/2}\right)$ differ by $\sim 3\%$. Sinha and Bardsley (1976) studied the difference in the cross sections for $^2P_{3/2}$ and $^2P_{1/2}$ ions of Kr^{+} at thermal energies, and showed that the reduced zero-field mobilities may be explained by similar differences in the charge transfer cross sections for the two states. Nikulin and Guschina (1978) computed the molecular–orbital correlation diagram for the Kr_2^{+}–Kr system. They considered a method for calculating the correlation diagrams of many-electron systems based on the exact solution of the two-centre problem with an effective parametric potential, took into account the electron screening of the nuclei as a quasi-molecule and allowed for the separation of the variables in the Schrödinger equation, in prolate spheroidal coordinates. Antar and Kessel (1984) measured the final charge states of the scattered ions and the inelastic energy losses for single collision of 0.25–3.0 MeV Kr ions with Kr. Their results show the impact-parameter dependence of several inner-shell excitations. Despite the amount of study that charge exchange of Kr^{+} with Kr has received, there is still doubt as to the magnitude of the cross sections. There has also been no previous work on the relationship of the differential cross section (DCS) for this reaction and the electronic state of the projectile. From theoretical considerations the DCS could have a strong dependence on the projectiles' degree of excitation.

0953-4075/99/020189+08$19.50

This paper reports measurements of the absolute differential and total cross sections for the production of Kr^{2+} and Kr^0 particles in Kr^+–Kr collisions in the energy range from 1.0 to 5.0 keV and in the laboratory angular scan from -4.0° to 4.0°.

2. Experiment

The experiments were carried out at the low-energy accelerator of Laboratorio de Cuernavaca, Instituto de Física, Mexico. A detailed description of the experimental approach has been given in a previous paper (Martínez 1998). Briefly, the Kr^+ ions formed in an arc discharge source containing Kr gas (99.99% purity) at ion source pressures of 0.04–0.07 mtorr were accelerated to 1.0–5.0 keV, and selected by a Wien velocity filter. The Kr^+ ions were then allowed to pass through a series of collimators before entering the gas target cell. The target cell was located at the centre of a rotatable, computer-controlled vacuum chamber that moved the whole detector assembly which was located 47 cm away from the target cell. A precision stepping motor ensured a high repeatability in the positioning of the chamber over a large series of measurements. The detector assembly consisted of a Harrower-type parallel-plate analyser (Harrower 1955) and two channel-electron multipliers (CEMs) attached to its exit ends. The neutral beam (Kr^0) passed straight through the analyser and impinged on a CEM so that the neutral counting rate could be measured. Separation of charged particles occurred inside the analyser, which was set to detect the Kr^{2+} ions with the lateral CEM. The CEMs were calibrated *in situ* with low-intensity Kr^0 and Kr^{2+} beams, which were measured as a current in a Faraday cup by a sensitive electrometer. The uncertainty in the detector calibration was estimated to be less than 3%. A retractable Faraday cup was located 33 cm away from the target cell, allowing the measurement of the incoming Kr^+ ion-beam current.

During the laboratory angular distribution experiment, the collimator in front of the lateral CEM was an orifice of 1 cm in diameter. Under the thin target conditions used in this experiment, the differential cross sections for the Kr^{2+} and Kr^0 formation were evaluated from the measured quantities by the expression

$$\frac{\mathrm{d}\sigma(\theta)}{\mathrm{d}\Omega} = \frac{I_\mathrm{f}(\theta)}{I_0 n l} \tag{1}$$

where I_0 is the number of Kr^+ ions incident per second on the target (typically $\sim 2.1 \times 10^9$ particles/s for the Kr^{2+} experiment and $\sim 2.2 \times 10^8$ particles/s for the Kr^0 experiment); n is the number of Kr atoms per unit volume (typically 1.2×10^{13} atoms/cm^3); l, the length of the scattering chamber ($l = 2.5$ cm) and $I_\mathrm{f}(\theta)$, the number of Kr^{2+} (or Kr^0) particles/(sr s) detected at a laboratory angle θ with respect to the incident beam direction (typically 1.3×10^8 particles/(sr s) for Kr^{2+} and $\sim 6.6 \times 10^{10}$ particles/s for Kr^0). The total cross section σ for the production of the Kr^{2+} and Kr^0 particles was obtained by the integration of $\mathrm{d}\sigma/\mathrm{d}\Omega$ over all angles; that is

$$\sigma = 2\pi \int_0^\pi \frac{\mathrm{d}\sigma}{\mathrm{d}\Omega} \sin(\theta)\, \mathrm{d}\theta. \tag{2}$$

Extreme care was taken when the absolute differential cross section was measured. The reported value of the angular distribution was obtained by measuring it with and without gas in the target cell with the same steady beam. Then point-to-point subtraction of both angular distributions was carried out to eliminate the counting rate due to neutralization of the Kr^+ beam on the slits and those arising from background distributions. The Kr^+ beam intensity was measured before and after each scan. Measurements not agreeing to within 5% were discarded. Angular distributions were measured on both sides of the forward direction to ensure they were

symmetric. The estimated rms error is 15%, while the total cross sections were reproducible to within 10% from day to day.

Several runs were made at different gas target pressures and $d\sigma/d\Omega$ was determined for each run. These were compared in order to estimate the reproducibility of the experimental results as well as to determine the limits of the 'single-collision regime' since the differential and total cross sections reported are absolute.

In the present work changes were not observed in the absolute values with respect to the ion source conditions. Also, no variation in the distributions were detected over a target pressure range of 0.2–0.6 mtorr.

Several sources of systematic errors are present and have been discussed in a previous paper (Martínez 1998). The absolute error of the reported cross sections is believed to be less than $\pm 15\%$. This estimate represents both random and systematic errors. The relative accuracy or reproducibility is found to be better than 15% for single-electron loss and 10% for single-electron capture.

3. Results and discussion

Measurements of differential cross sections (DCSs) have been performed at laboratory angles of $-4^{\circ} \leqslant \theta \leqslant 4^{\circ}$ and collision energies of $1.0 \leqslant E_{\mathrm{lab}} \leqslant 5.0$ keV.

3.1. For single-electron loss

Figure 1 exhibits the angular and energy dependence (the reduced differential cross section $\rho = (d\sigma/d\Omega)\theta \sin\theta$) of the single-electron loss differential cross sections in the laboratory

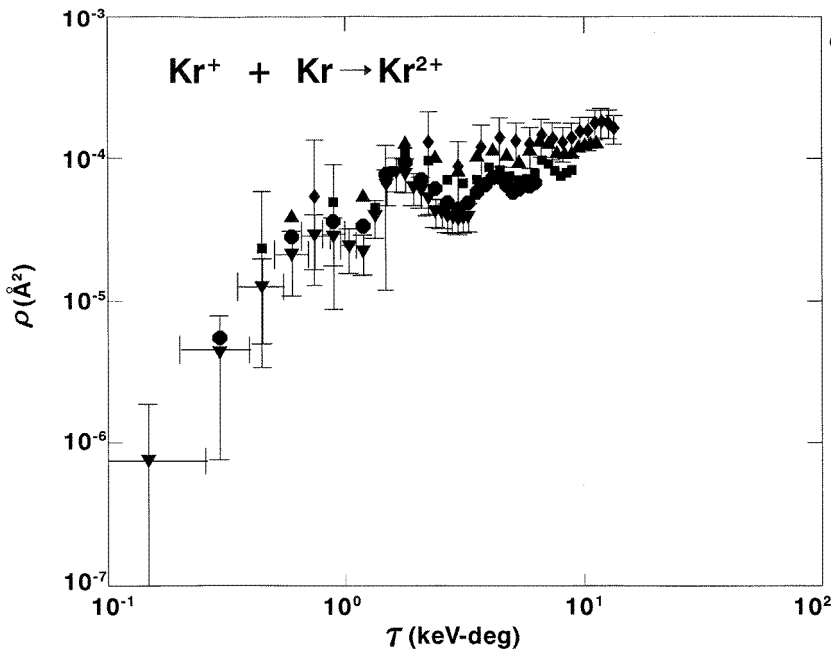

Figure 1. Reduced differential cross sections for single-electron loss of Kr^{+} ions in Kr. ▼, 1.0 keV; ●, 2.0 keV; ■, 3.0 keV; ▲, 4.0 keV; ♦, 5.0 keV.

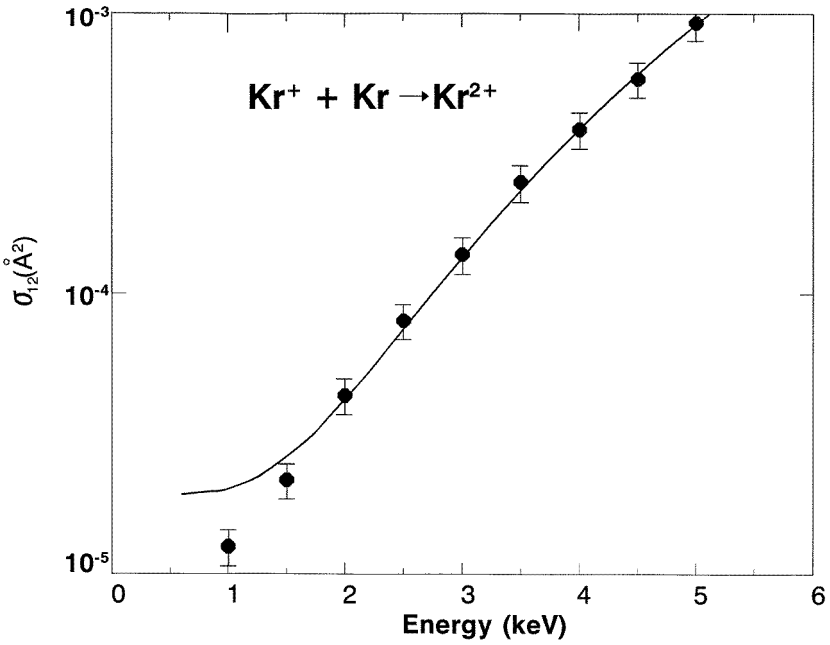

Figure 2. Total cross sections for single-electron loss of Kr^+ ions in Kr. ●, present measurements. The full curve represents a least-squares fit of a power function.

Table 1. Cross sections for single-electron loss and capture of Kr^+ on Kr.

Energy (keV)	σ_{10} (Å^2)	σ_{12} (10^{-4} Å^2)	σ_{10}/σ_{12}
1.0	0.41 ± 0.04	0.12 ± 0.02	32 800.00
1.5	0.63 ± 0.06	0.22 ± 0.03	29 302.33
2.0	1.00 ± 0.10	0.43 ± 0.06	23 255.81
2.5	1.40 ± 0.14	0.80 ± 0.12	17 500.00
3.0	1.57 ± 0.16	1.38 ± 0.21	11 376.81
3.5	1.78 ± 0.18	2.50 ± 0.38	7 120.00
4.0	1.98 ± 0.20	3.84 ± 0.58	5 156.25
4.5	2.21 ± 0.22	5.80 ± 0.87	3 810.35
5.0	2.29 ± 0.23	9.25 ± 1.39	2 475.68

system, where the abscissa is the reduced angle $\tau = E_{\text{lab}}\theta$. For clarity, in figure 1 horizontal error bars were put only on some data. The curves representing the reduced differential cross sections (RDCS) for the different energies show the following behaviour. The RDCS have an overall increase of two orders of magnitude. A maximum, independent of energy, is present at 0.8 keV deg and is followed by an oscillatory behaviour. The general behaviour for these processes can be approximated by common curves at the energies studied (Smith *et al* 1966, 1967). The measured differential cross sections for single-electron loss of Kr^+ impact on Kr have been integrated over the observed angular range, and are shown in figure 2 and listed in table 1. The error bars are a measure of the reproducibility of the data (15%). Our cross sections are found to be of the order of 10^{-20} cm^2. The full curve in figure 2 represents a least-squares fit of a power function using the present data ($\sigma_{12} = \left(0.189 + 0.0143E^4\right) \times 10^{-20}$ cm^2, with E in keV, and a correlation coefficient of 0.998 46). The shape of the total cross section shows a

rapid monotonically increasing behaviour as a function of the incident energy. This behaviour can be explained qualitatively in terms of momentum transfer and projectile–target interaction time. For energies smaller than E_{max} (the energy at which the cross section is maximum) a smaller momentum can be transferred to the projectile electrons as the energy of the projectile decreases (Atan *et al* 1991). From the least-squares fit we find that $\sigma_{12} \sim E^4$ in the present energy range. A similar behaviour was found by Martínez (1998) for single-electron loss cross section measurements of Ar^+ ions colliding with He where $\sigma_{12} \sim E^2$ in the same energy range. Kaneko (1985), using the unitarized impact parameter method to calculate the electron loss cross section for He^+ ions colliding with He, N_2, Ar and Kr, found that $\sigma_{12} \sim E^{2.8}$ in the energy range $30 \leqslant E \leqslant 150$ keV; no remarkable differences in the energy dependence of σ_{12} could be found for any atom. We know that these are different collision systems but can be used to make a comparison of the behaviour of the cross sections as a function of the impact energy. The difference in the energy dependence of the present data, Martínez's 1998 results and Kaneko's 1985 calculations can be explained by considering that in ion–atom collisions, the interaction probabilities are strongly influenced by the electronic structures of the exciting partner and projectile; the Kaneko (1985) calculation gives a better agreement with the data, in the region where the impact velocity $v \sim Z_1 v_0$ (Z_1 is the atomic number of the projectile and v_0 is the Bohr velocity) as well as for hydrogen-like ions.

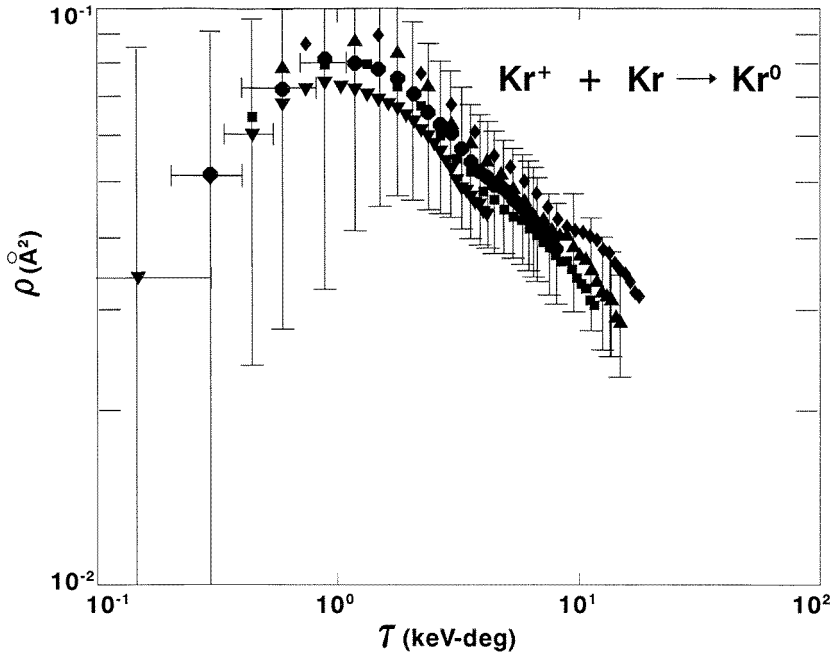

Figure 3. Reduced differential cross sections for single-electron capture of Kr^+ ions in Kr. ▼, 1.0 keV; ●, 2.0 keV; ■, 3.0 keV; ▲, 4.0 keV; ♦, 5.0 keV.

3.2. For single-electron capture

Characteristic reduced differential cross sections for single-electron capture of Kr^+ ions in Kr for different values of the incident energy are presented in figure 3. For clarity, in figure 3

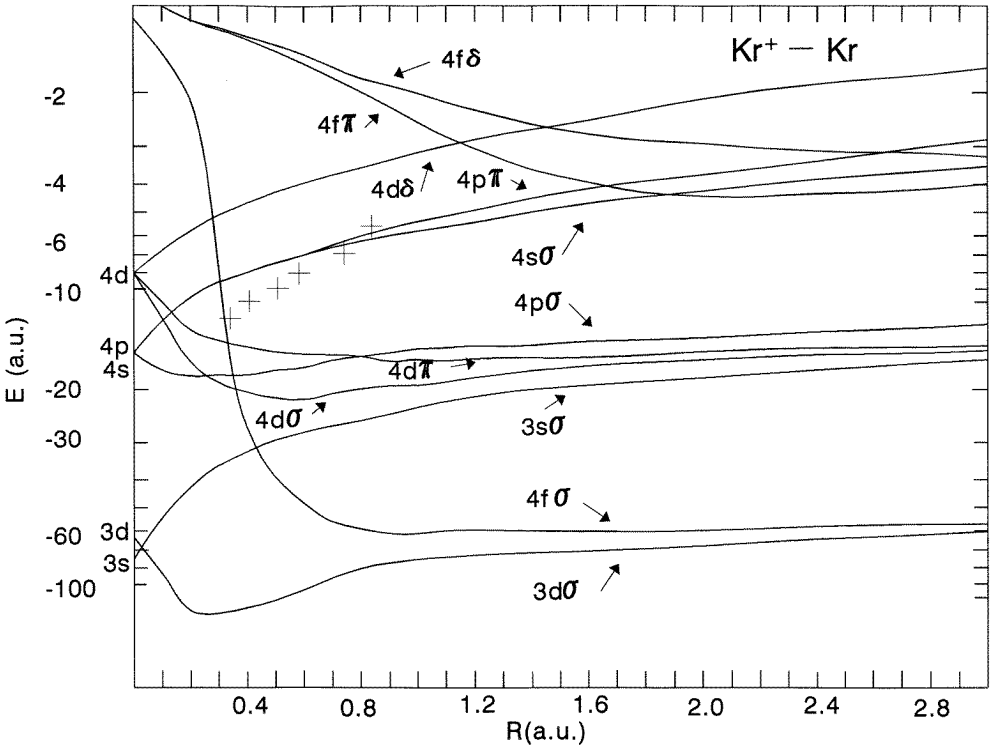

Figure 4. MO correlation diagram of the system Kr_2^+ (taken from Nikulin and Guschina 1978). Crosses indicate the trend of the orbital obtained from the experimental data of Afrosimov *et al* (1976).

the horizontal error bars were only put on some data. Several remarkable features can be observed which are worth pointing out: (a) $\rho(\tau)$ shows a similar behaviour at all energies within the experimental uncertainty; (b) it increases slowly up to 1.2 keV deg by less than an order of magnitude. This is followed by a hump structure and a linear decrease beyond 2 keV deg. The features that occur at the same value of τ for different energies indicate that they originate in a common region of the interaction potential, since constant τ implies nearly constant impact parameter and distance of closest approach (Smith *et al* 1966, 1967). In this particular case, the impact parameter b was evaluated using an exponentially shielded Coulomb potential (Smith *et al* 1966, 1967). The maximum independent of the collision energy is around 1.2 keV deg (which corresponds to an impact parameter of $b \approx 1.671\ a_0$). It is conceivable that this crossing radius corresponds to $4f\pi$–$4p\pi$ crossings of the MO correlation diagram of the system Kr^+ (Nikulin and Guschina 1978), which has a value of 1.7 a_0 (see figure 4). Notice that the value of the crossing radius obtained from the RDCSs is far from the other closest crossings radius (1.5 and 2.0 a_0), which correspond to $4f\delta$–$4d\delta$ and $4f\pi$–$4s\sigma$ crossings, respectively (see figure 4). Plotted in figure 5 and listed in table 1 are the total cross sections for single-electron capture obtained by integration of the angular distributions as a function of the impact energy. The error bars are a measure of the reproducibility of the data (10%). The σ_{10} appear to be approaching a maximum value at a rather lower energy than σ_{12} and increase slowly as the incident energy is increased. For many years this has been of considerable interest in symmetric charge-transfer reactions at low energies. Also, a simple theoretical model of

the process has been developed, where the results can be expressed in the form (Sinha and Bardsley 1976)

$$\sigma^{1/2} = k_1 - k_2 \ln(E) \tag{3}$$

where σ is the cross section expressed in Å^2, E is the energy of the ions in keV, and k_1 and k_2 are constants, which are determined mainly by the ionization potential of the atom involved in the collision.

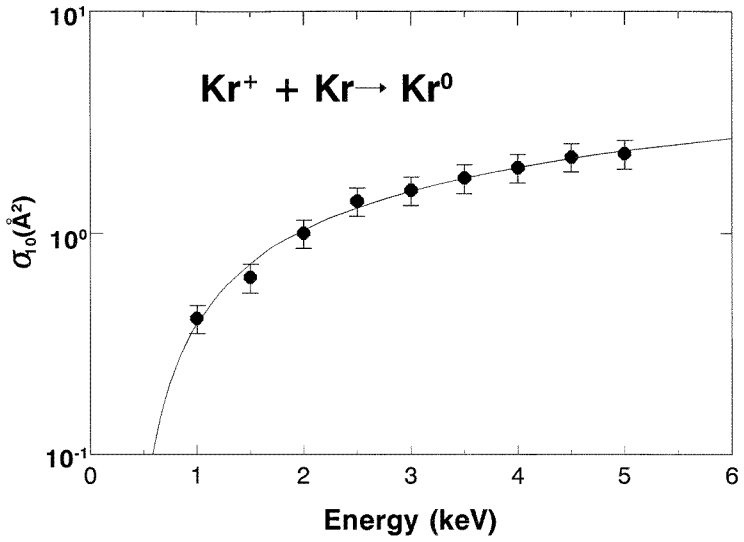

Figure 5. Total cross sections for single-electron capture of Kr^+ ions in Kr. ●, present measurements. The full curve represents a simple theoretical model (see text).

The cross section function can be represented by the expression $\sigma^{1/2} = (0.620\,645 + 0.567\,905 \ln E)$ Å, which was obtaining with a least-squares fit. The impressive agreement between the present data and equation (3) may be fortuitous, but the difference is better than 5% over the present energy range.

The loss and capture processes are opposite: the former increases the charge on the ions, and the latter decreases it. In this case, the value of σ_{10} is four orders of magnitude greater than the value of σ_{12} (see table 1). If we assume that $\sigma_{10} \approx \pi b_c^2$ and $\sigma_{12} \approx \pi b_L^2$, where b_c and b_L are the mean values of the impact parameters for the collision, make the major contribution to the cross section of capture and loss, respectively, then we can estimate σ_{10}/σ_{12}. Consequently, under this model there is a greater value of the mean impact parameter for electron capture than for electron loss; one can observe no decrease in the capture cross section. Also, with increasing energy the ratio σ_{10}/σ_{12} decreases, indicating that a higher impact energy favours reactions with larger energy defect. This fact has already been ascertained in similar experiments (Huber 1975, 1976, Siegel *et al* 1972).

The major results of this investigation are summarized below:

(a) Experimental observations of the absolute total cross sections for single-electron loss and capture of Kr^+ in Kr at impact energies between 1.0 and 5.0 keV have been reported.

(b) The reduced differential cross sections for single-electron loss show a maximum at a value of $\tau \approx 0.8$ keV deg.

(c) The reduced differential cross sections for single-electron capture present a maximum at a value of $\tau \approx 1.2$ keV deg, which suggests the existence of a curve crossing at $R_c = 1.67\ a_0$. It is conceivable that this crossing radius corresponds to $4f\pi$–$4p\pi$ crossing of the MO correlation diagram of the system Kr_2^+. It thus appeared desirable that a detailed theoretical analysis be carried out to confirm this critical transition region around $R_c = 1.67\ a_0$.

(d) For single-electron loss, the cross sections are found to have an order of magnitude of 10^{-20} cm^2 and show a rapid monotonically increasing behaviour as a function of the incident energy.

(e) The shape and magnitude of the present total cross sections for single-electron capture are in good agreement with a simple theoretical model over the entire energy range of the present study.

(f) A larger set of experimental cross sections is now available at low-keV energies, for electron loss and capture of Kr^+ in Kr.

Acknowledgments

We are grateful to B E Fuentes for helpful suggestions and comments, and to P G Reyes and A González for their technical assistance. Research supported by DGAPA IN-100392 and CONACyT 3659P-E9607.

References

Afrosimov V V, Gordeev Yu S, Zinoviev A N, Rasulov D N and Shergin A P 1976 *Zh. Eksp. Teor. Phys.* **24** 33–6
Antar A A and Kessel Q C 1984 *Phys. Rev.* A **29** 1070–8
Atan H, Steckelmacher W and Lucas M W 1991 *J. Phys. B: At. Mol. Opt. Phys.* **24** 2559–69
Barat M, Baudon J, Abignoli M and Houver J C 1970 *J. Phys. B: At. Mol. Phys.* **3** 230–50
Harrower G A 1955 *Rev. Sci. Instrum.* **26** 850–4
Helm H 1976 *J. Phys. B: At. Mol. Phys.* **9** 2931–43
Huber B 1975 *Z. Phys.* A **275** 95–101
——1976 *Z. Phys.* A **277** 31–3
Kaneko T 1985 *Phys. Rev.* A **32** 2175–85
Martínez H 1998 *J. Phys. B: At. Mol. Opt. Phys.* **31** 1553–62
Nikulin V K and Guschina M A 1978 *J. Phys. B: At. Mol. Phys.* **11** 3553–62
Sinha S and Bardsley J N 1976 *Phys. Rev.* A **14** 104–13
Smith F T, Marchi R P, Aberth W, Lorents D C and Heinz O 1967 *Phys. Rev.* **161** 31–46
Smith F T, Marchi R P and Dedrick K G 1966 *Phys. Rev.* **150** 79–92
Siegel M W Chen Y H and Boring J W 1972 *Phys. Rev. Lett.* **28** 465–70